Research Square

Preprints are preliminary reports that have not undergone peer review.
They should not be considered conclusive, used to inform clinical practice,
or referenced by the media as validated information.

Sustained Formation, Movement and Destruction of Complex Coacervates in a Waste-Less System Driven by Electricity

Guillermo Monreal Santiago

monrealsantiago@unistra.fr

Université de Strasbourg

Svetlana Samokhvalova

Université de Strasbourg

Kalliopi Fourli

Université de Strasbourg

Luis Calahorra Río

IMDEA-Nanociencia

Article

Keywords:

Posted Date: July 30th, 2025

DOI: https://doi.org/10.21203/rs.3.rs-7067361/v1

License: This work is licensed under a Creative Commons Attribution 4.0 International License.
Read Full License

Additional Declarations: There is **NO** Competing Interest.

Version of Record: A version of this preprint was published at Nature Communications on August 27th, 2026. See the published version at https://doi.org/10.1038/s41467-026-77229-1.

Sustained Formation, Movement and Destruction of Complex Coacervates in a Waste-Less System Driven by Electricity

Svetlana Samokhvalova[1], Kalliopi Fourli[1], Luis Calahorra Río[2], Guillermo Monreal Santiago[1]*

1- UMR7140 – Chimie de la Matière Complexe, Université de Strasbourg, CNRS, 4 Rue Blaise Pascal, 67081 Strasbourg, France

2- IMDEA-Nanociencia, Faraday 9, 28049, Madrid, Spain

E-mail: monrealsantiago@unistra.fr

Abstract: Transient compartmentalization and directional motion are key elements of living matter, and milestones in the development of complex chemical systems such as protocells. Coacervate droplets have been proposed as compartments in this context, as they share properties with biomolecular condensates, which act as transient compartments in biology. Previous efforts to develop out-of-equilibrium coacervates use exergonic reactions as an energy source, but this leads to the accumulation of the side-products of the driving reaction, preventing operation over long periods of time. Here, we present a novel strategy to drive the transient formation and movement of coacervate compartments, using an electric potential between two electrodes as an energy source. In this system, the electrochemical oxidation of a cysteine-containing peptide increases its multivalency, leading to complexation with a polyanion and coacervate formation at the anode. The electrochemically-formed coacervates then move by electrophoresis over a distance more than three orders of magnitude larger than their diameter. In the proximity of the cathode, an electrocatalytic cycle dissolves the coacervates by reduction, recovering the free peptide and polyanion, which can diffuse back to the anode and react again. The system reaches a steady state, in which coacervates are simultaneously forming, moving, and disappearing in different regions of the cell. Since no side-products are generated, the formation-movement-destruction regime can be sustained for more than 16 hours, (two orders of magnitude longer than the lifetime of individual droplets), reaching a steady state. This combination of transient formation, directional movement and coacervate compartments is unique, and can be used for electricity-driven active transport.

Introduction

Transient compartmentalization is a fundamental step in the development of complex systems with emergent, life-like properties.[1,2] Spatially segregating some of the components in a chemical reaction network can lead to multiple non-equilibrium regimes,[3] or to different outcomes in a community of replicators and parasites.[4] Transient compartmentalization can also be coupled to directional movement to transport chemicals against a chemical gradient. Biological examples of this are endo- and exocytosis, forms of active transport in which molecules move against a gradient by transient encapsulation into moving vesicles.[5,6]

In the cell, compartmentalization often takes place in membraneless organelles (MLOs), liquid droplets that form due to the interactions between proteins, nucleotides, and other biomolecules.[7–9] MLOs are involved in a variety of cellular processes, from RNA metabolism to protein synthesis. A common feature among some MLOs is that they are active matter: they consume energy from chemical reactions, resulting in their transient formation, movement, aging, or dissolution in response to certain stimuli, or after a period of time.[10,11]

Complex coacervates have often been used as synthetic mimics of MLOs.[12–14] Coacervates form in an aqueous solution of polymers, via spontaneous liquid-liquid phase separation (LLPS). This process is driven by attractive interactions (usually electrostatic), as well as counterion dilution.[15,16] Complex coacervate droplets have been shown to encapsulate molecules,[17,18] accelerate chemical reactions,[19] or control the aggregation of proteins,[20] similarly to their biological counterparts.

There has been a significant effort to prepare coacervates in an out-of-equilibrium regime, in order to mimic the active nature of MLOs,[21,22] or to develop synthetic protocells.[23–26] For instance, the groups of Keating,[21] Spruijt,[27] and Dhiman[28] have shown timed and/or transient coacervate formation by reversible enzymatic phosphorylation. Walther et al. have demonstrated transient formation of DNA-based coacervates by strand hybridization and dissociation with a cross-linking nucleic acid that controls multivalency of the DNA strand.[29] Boekhoven et al. have used chemical fueling to achieve transient coacervate formation,[22,30] non-equilibrium shell formation,[31] and in a recent preprint, movement.[32] Finally, our group has recently shown a new strategy to trigger delayed coacervate formation and changes in coacervate properties over time, based on the decomposition of a volatile salt.[33] The design of chemically-fueled coacervates is limited by their sensitivity to waste production.[27] Over time, the products

of the driving reaction build up, reaching a concentration in which they have a non-desirable effect on the reaction network. This problem is not exclusive of coacervates: practically all systems that are driven by an exergonic reaction tend to be affected from waste accumulation, limiting for how long they can be operated,[34] or requiring a mechanism that removes the waste-products from the medium.[31,33,35]

An alternative approach to create waste-less active systems is to use an electric potential as a driving force.[36] In a recent example, Guan and coworkers[37] have used this strategy to drive supramolecular polymerization through two redox reaction cycles. Their system is based on a thiol building block, which is soluble as a monomer but self-assembles into fibers when oxidized to a disulfide. By introducing two electrodes in the solution, the oxidation and reduction of the building block can take place at the same time but spatially separated from each other, causing assembly in the proximity of one electrode and disassembly next to the other. Since the two redox cycles only involve the transfer of electrons, and no net products are generated or consumed in the overall reaction, the system can maintain a steady state of self-assembly/disassembly for at least 4 hours with the electric potential as the only energy input.

We hypothesized that a similar strategy could be used to drive the formation of coacervates in an out-of-equilibrium regime. Two recent reports have shown that complex coacervates can be reversibly formed upon chemical oxidation or reduction.[38,39] In both cases coacervation was driven by an increase in the multivalency of one or both oligoelectrolytes. Particularly, Li et al. have shown that the oxidation of a cysteine-containing charged peptide can trigger the formation of a complex coacervate,[39] as the corresponding disulfide-linked dimer contains twice as many charges as the monomer. Even without redox-sensitive functional groups, the coacervate phase is susceptible to electric potentials due to its high charge density. Strong electric fields (> 10 V/cm) have been shown to disrupt the internal structure of coacervates,[40] or trigger an exchange between polyelectrolytes.[41] Weaker electric fields (1-10 V/cm) do not have such an effect, but they can instead cause electrophoretic movement, which magnitude and direction depend on the surface charge of the coacervates.[42–44]

Here, we report the first example of an electricity-driven system, in which the formation, movement, and destruction of complex coacervates are driven only by the difference in electric potential between two electrodes (Figure 1). Our system continuously produces coacervate droplets thanks to the anodic oxidation of a cysteine-containing peptide. These droplets then migrate over several millimeters to the cathode, where they are dissolved after an electrocatalyst-mediated reduction. The system is completely waste-free, and a continuous formation-movement-destruction regime can be maintained for longer than 16 hours.

Results and Discussion

Electrochemical Oxidation and Coacervate Formation

We designed our system around a tetrapeptide (KKKC), containing three positively charged lysines and a cysteine (Figure 1). Cysteine acts as the redox-responsive functionality: when oxidized to a disulfide, the peptide will be dimerized to $(KKKC)_2$, a molecule with twice as many charges, and in principle, a higher propensity to form coacervates (Figure 2a).

First, we explored the oxidation of KKKC and its effect on coacervate formation. Mixing KKKC with either pAA or ATP did not lead to coacervate formation in our experimental conditions. When KKKC was oxidized by the addition of $NaBO_3$, the solution containing pAA became turbid, and we could observe the formation of coacervates by optical microscopy (Figure 2b). On the other hand, the sample containing ATP did not form coacervates even after oxidation, indicating that complexation is less favorable in this case due to the lower multivalency of ATP. Having confirmed that coacervation can be triggered by the chemical oxidation of KKKC, we studied if the same could be achieved electrochemically. For this, we prepared an undivided cell by introducing flat silver electrodes in a solution containing KKKC and pAA, and applied an external potential with a commercial power supply.[45] As soon as the potential was applied, we observed the formation of coacervate droplets close to the surface of the anode (Figure 2c). No droplets were observed in absence of either pAA or KKKC, confirming that these droplets were indeed the result of complex coacervation (Figure S1). We used Ellman's test (Figure S2) and ^{1}H-NMR spectroscopy (Figure S3) to characterize their chemical composition, revealing that electrochemical oxidation also results in thiol oxidation and the formation of a disulfide dimer. Previous reports have shown that cysteine derivatives are difficult to oxidize on the surface of solid electrodes.[46–48] Particularly, Guan and coworkers did not observe the formation of disulfides on a glassy carbon electrode (GCE), only detecting irreversible oxidation at high potentials.[49] This was also the case for KKKC, for which we could not detect any electrochemical response by cyclic voltammetry (CV)

when using a GCE as a working electrode (Figure S4). On the other hand, when the working electrode was changed to silver, we detected a broad anodic peak corresponding to the oxidation of thiols to disulfides at 160 mV (Figure S5), consistent with our observations in the undivided cell. The reverse reaction could also be observed, as a broad reduction peak between -0.3 and -0.1 V. We ascribe the difference between the two electrodes to the high affinity of thiols for silver.[50–52]

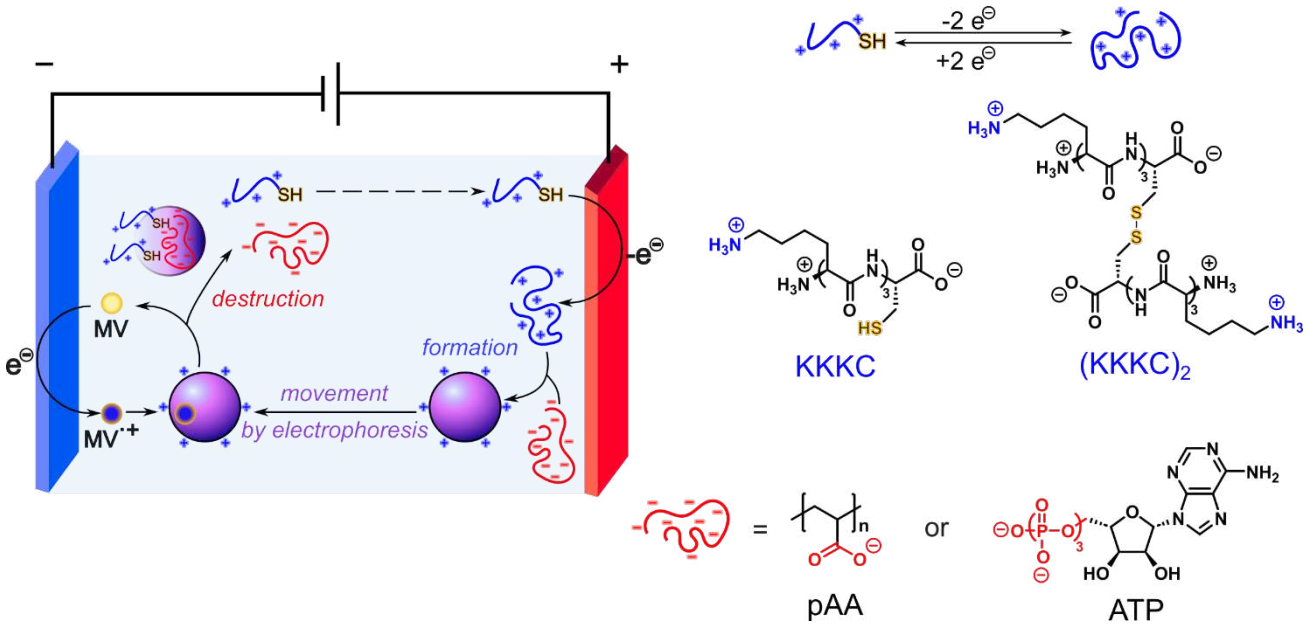


Figure 1. General scheme showing the electricity-driven formation, movement and destruction of $(KKKC)_2$-based coacervates. The thiol group of the KKKC is oxidized at the anode to form a disulfide-bearing dimer $(KKKC)_2$. The increase in the multivalency of the oligocation leads to its complexation with pAA or ATP, and to the formation of complex coacervates in the proximity of the anode. These coacervate droplets then move by electrophoresis towards the cathode. There, an electrocatalytic cycle mediated by MV leads to the reduction of $(KKKC)_2$, dissolving the coacervates and recovering KKKC and the polyanion, which then diffuse back to the anode and participate again in coacervate formation.

Surprisingly, the KKKC/ATP system also formed coacervates upon electrochemical oxidation (Figure 2c), even if it did not when oxidized with $NaBO_3$. This difference is probably due to the side-products of the chemical oxidation: the reaction between $NaBO_3$ and cysteine produces borate salts, which increase the ionic strength of the solution, weakening electrostatic interactions. In the $(KKKC)_2$/ATP system, the electrostatic interactions between oligocation and oligoanion are already weak since both components are oligomeric, so this increase in ionic strength is enough to prevent coacervate formation. On the other hand, when KKKC is oxidized at the anode, the ionic strength of the solution does not change, and coacervate formation can take place. This is an example of the difference between electricity- and chemically-driven systems: waste-products are accumulated in the latter, leading to unwanted effects. This is particularly important for the current system: since practically all complex coacervates dissolve at high ionic strengths, continuous coacervate formation could not be sustained in a system driven by oxidation with $NaBO_3$.

Coacervate Movement Driven by Electrophoresis

Coacervate droplets can move in electric fields by electrophoresis.[42,43] Both the direction and the velocity of this movement depend on the ζ-potential of the droplets, and thus on the ratio between positive and negative charges in the coacervates. To determine the relative charge of $(KKKC)_2$-containing coacervates and optimize their speed in this system, we tracked the movement of the electrochemically-formed coacervates in the electric field created between the two electrodes (Figure 3, Supplementary Video 1). When KKKC and pAA were mixed in a stochiometric charge ratio (1:1) and an electric field of 0.95 V/cm was applied (0.7 V, 0.74 cm), the coacervates moved towards the cathode with a constant speed of ~1 μm/s, indicating that their overall charge was slightly positive but close to neutral. When KKKC was added in excess (2.5:1 charge ratio), their speed increased to 12.5 μm/s, and the droplets reached the cathode in ca. 10 minutes. This confirmed that the movement of the coacervates was mainly driven by electrophoresis, and that the non-stochiometric mixing ratio between precursors was translated to a charge imbalance in the composition of the coacervates. For the systems containing ATP as the oligoanion, a 1:1 mixing ratio resulted in negatively-charged droplets (Figure S6), consistent with other ATP-containing coacervates.[42] These droplets initially moved away from the anode due to droplet-droplet repulsion, but after an initial displacement they started moving back towards it. This resulted in a fixed front of coacervates that

remained ~30 µm away from the electrode surface. Increasing the amount of KKKC in this system resulted in positively-charged coacervates that moved towards the cathode, but still at a slower speed than in the system containing pAA. In general, these results show that there is a direct relationship between the composition of coacervates and their movement speed. Therefore, the mixing ratio between polycation and polyanion can be used

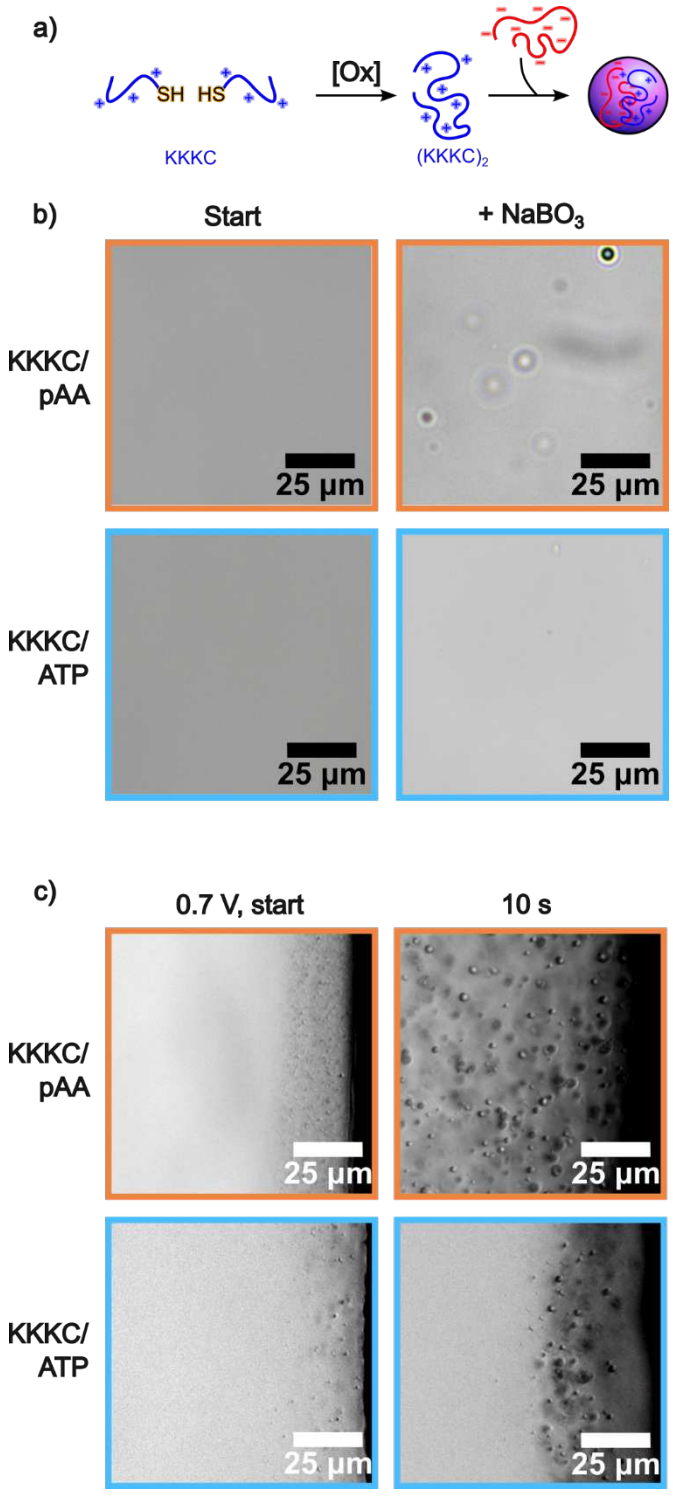


Figure 2. Coacervate formation triggered by the chemical or electrochemical oxidation of KKKC. a) General scheme showing oxidation and coacervate formation in presence of a suitable oligo- or polyanion. b) Micrographs of solutions containing KKKC and either pAA or ATP, before and after chemical oxidation (with 1.2 eq. of $NaBO_3$). c) Micrographs recorded next to the anode in a solution containing KKKC and either pAA or ATP, immediately after the application of an electrical potential (0.7 V) and after 10 seconds. Note that the KKKC/ATP system forms coacervates when oxidized electrochemically but not after reaction with $NaBO_3$, due to the ionic side-products formed in the latter. [KKKC] = [ATP] = 1.34 mM, [pAA] = 4 mM (in monomer units) [NaCl] = 100 mM in the samples with pAA, 10 mM in the samples with ATP. The size of scale bars is 25 µm.

to control the lifetime of the droplets: since coacervate destruction only takes place in the proximity of the cathode (see below), slower coacervates will have a longer lifetime and vice-versa.

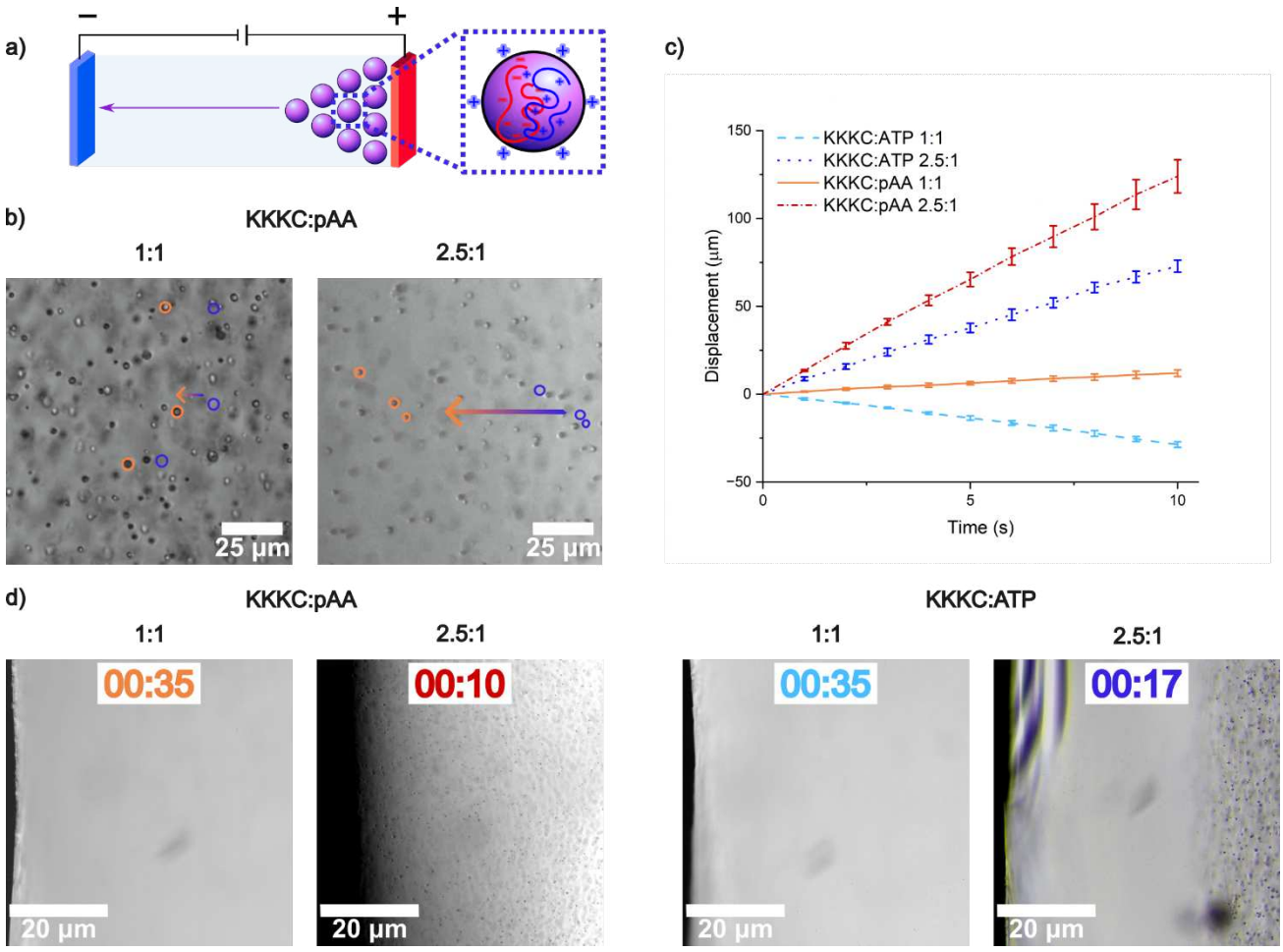


Figure 3. Electrophoretic movement of $(KKKC)_2$-based coacervates in an electric field. a) Scheme showing the movement of positive coacervates from the anode to the cathode. b) Micrographs of electrochemically formed $(KKKC)_2$/pAA coacervates with different ratios between positive and negative charges. The displacement of different droplets was measured over time: the blue circles represent their initial position, and the orange ones their position after 10 s. c) Displacement over time of coacervate droplets with different compositions. Each point represents the average displacement of five droplets, and the error bars represent the standard deviation. Positive displacement values indicate movement towards the cathode. d) Micrographs of the area next to the cathode for coacervates with different compositions, at specific times after the application of the electric potential. The strength of the electric field in all the measurements is 0.95 V/cm (voltage = 0.7 V). The initial concentrations are [ATP] = 1.34 mM, [pAA] = 4 mM (in monomer units) [KKKC] = 1.34 or 3.34 mM (for 1:1 or 2.5:1 charge ratios, respectively). [NaCl] = 100 mM in the samples with pAA, 10 mM in the samples with ATP. The size of the scale bars is indicated in the pictures. Times are reported as hh:mm.

Coacervate Destruction

Keeping a constant electric potential for longer than 10 minutes led to a continuous flow of coacervate droplets reaching the cathode. Even though we could not monitor the behavior of these droplets on the surface of the electrode (due to the latter blocking the light in our setup), we could detect their coalescence by the formation of a continuous coacervate phase in the bottom of the cell (Figure S7). While some droplets sink to the bottom of the cell through its entire length, the coalesced phase was distinctly propagating from the cathode, indicating that coacervates were accumulating in that area instead of reacting. In other words, the rate at which coacervates were dissolved by the electrochemical reduction of $(KKKC)_2$ was significantly slower than the rate at which they formed and reached the cathode. We hypothesize that this accumulation is caused by a difference in reaction rates between oxidation and reduction: while KKKC is soluble and its thiol group is easily accessible, most of the $(KKKC)_2$ that reaches the cathode is in the form of coacervates, which potentially shield the disulfides from reaching the surface of the electrode. We confirmed this hypothesis by CV (Figure S8): while the peak corresponding to the oxidation of KKKC was practically identical in presence or in absence of pAA, the current corresponding to disulfide

reduction was significantly smaller when pAA was added. This indicates that a significant fraction of disulfides is unavailable for reaction when coacervates are formed.

In order to facilitate the reduction of $(KKKC)_2$ and the dissolution of coacervates, we used methyl viologen (MV) as an electrocatalyst. Methyl viologen is an organic divalent cation that can be reduced to the radical cation $MV^{\cdot+}$, which in turn reacts with disulfides, reducing them chemically.[37] Since $MV^{\cdot+}$ is small and relatively stable, it can diffuse in and out of the coacervates, reacting with $(KKKC)_2$ and regenerating MV and KKKC (Figure 4a). We tested this reaction by CV (Figure 4b, Figure S9 and Figure S10). In presence of coacervates, a new cathodic peak appeared for MV at -594 mV, a slightly lower potential than its reduction in water (-682 mV). We attribute this peak to the reduction of the MV molecules that are compartmentalized into the coacervates. Since the coacervate phase is relatively hydrophobic, the coacervate droplets can sequester MV from the solution, acting as a new solvent and changing the ΔG of the reduction.[19] The intensity of the peak increases with each cycle of oxidation and reduction, consistent with the formation of more coacervates on the surface of the electrode. While the reduction of free MV in water is reversible, the cathodic peak at -594 mV appears to be irreversible. This is consistent with a chemical reaction consuming $MV^{\cdot+}$ as soon as it is formed[37] – in this case, the reduction of $(KKKC)_2$.

Next, we confirmed that the MV-mediated reduction of $(KKKC)_2$ led to the dissolution of coacervates. For that, we prepared a sample containing KKKC, pAA, and MV, and generated coacervates by using a constant electric potential of 0.7 V. This potential already generates enough $MV^{\cdot+}$ to reduce $(KKKC)_2$ and enable the recirculation of material (as shown below), but to clearly visualize the effect, we waited until some coacervate droplets had settled on the bottom of the cell next to the cathode and applied a higher potential (1.5 V). As soon as this potential was applied, we observed a blue color next to the cathode, characteristic of the $MV^{\cdot+}$ radical cation (Figure 4c). The intensity of the color was significantly stronger within the coacervates than in the surrounding solution, indicating that the diffusion of $MV^{\cdot+}$ into the coacervate phase is a favorable process. Furthermore, the size of the coacervates decreased quickly after the application of the potential, confirming the MV-mediated reduction leads to the dissolution of the coacervates (Figure 4d).

Steady state

When the coacervates are dissolved, free KKKC and pAA can return to the anode (by diffusion or by convective flows generated by the movement of coacervates) and participate in oxidation and coacervate formation again. In this way, the system can be driven into a sustained formation-movement-destruction regime. We characterized this regime in two systems containing KKKC and pAA. Only one of the systems contained MV, enabling the regeneration and recirculation of coacervate precursors, while the other one was taken as a control with only the "forward" part of the cycle (Figure 5, Supplementary Video 2). For each system, we prepared two samples and studied them for a long period of time during the application of an electric potential, in one case monitoring the proximity of the anode and in the other one monitoring the proximity of the cathode.

In an initial stage, both systems were almost identical, and we could observe the formation of coacervates next to the anode followed by their migration towards the cathode (Figure 5a, Figure S11). The number of droplets forming next to the anode increased for the first hour before starting to decrease as KKKC and pAA were depleted. As expected, the same trend was observed on the cathode, albeit with a short delay due to the movement along the cell. Additionally, the droplet density was slightly lower at the cathode than at the anode, as some of the coacervates sank to the bottom of the cell along the way, leading to a loss of material.

After this initial period, the number of coacervates continued to drop quickly in the system without MV, until no more droplets could be observed after 5 h at the anode (Figure 5b) or 8.5 h at the cathode (Figure 5c). We took this point as the moment in which the concentration of KKKC next to the anode was too low for oxidation, and the reaction could not continue without the recirculation of material. In the case of the system containing MV, the number of coacervates also decreased initially, but it never stopped completely. On the contrary, the system reached a steady state after 6 h, with a constant number of coacervates being produced and destroyed at the two respective electrodes. This steady state could be maintained for at least another 10 h without any significant changes, for a total of more than 16 h of simultaneous formation, movement and destruction.

As described above, the transient formation and movement of coacervate droplets are particularly appealing because of their ability to compartmentalize and transport solutes. In order to test if the electrochemically-formed coacervates described in this work can be used as compartments, we incubated different fluorescent dyes in presence of electrochemically-generated $(KKKC)_2$/pAA and $(KKKC)_2$/ATP coacervates, and studied their partition by fluorescence microscopy (Figure S12 and Figure S13). Interestingly, the partition of the different dyes between solution and coacervate depends strongly on the chemical nature of the polyanion and the dyes, as well as the

charge ratio and the salt concentration: depending on these parameters, some dyes were concentrated inside of the coacervates while other were excluded almost completely. This result opens the door for using these coacervates as selective transporters, with a preference for compartmentalizing and moving some cargo molecules over others.

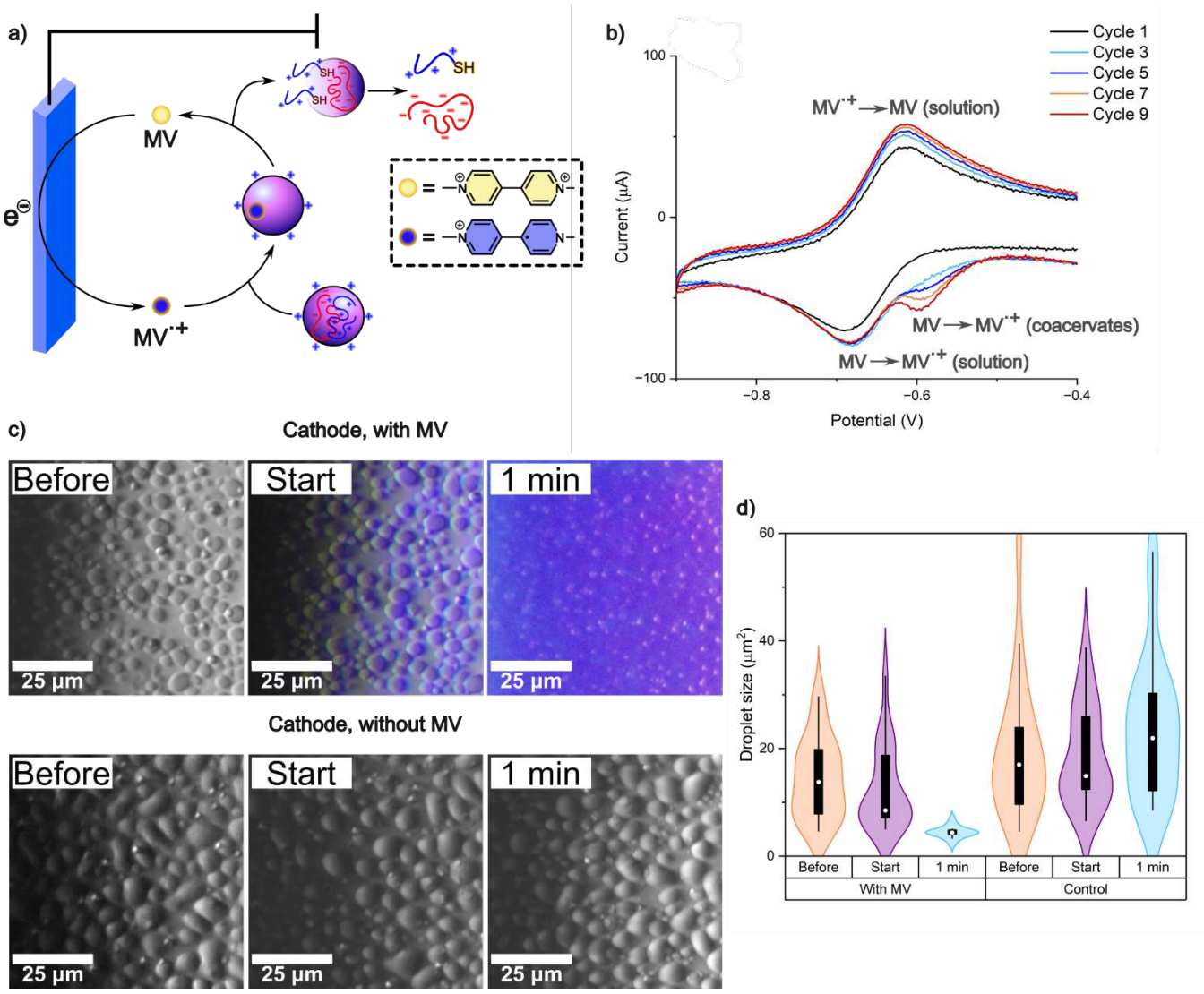


Figure 4. Destruction of $(KKKC)_2$/pAA coacervates using an electrocatalytic cycle. a) Scheme of the electrocatalytic cycle that results in the reduction of $(KKKC)_2$, with MV as an electrocatalyst. $MV^{\cdot+}$ is first generated in the surface of the cathode by electrochemical reduction of MV. Then, it diffuses inside of a coacervate droplet, where it can react with $(KKKC)_2$. This reaction regenerates MV and KKKC, and causes the dissolution of the coacervate. b) CV scans (Ag working electrode, vs Ag/AgCl) for a mixture containing $(KKKC)_2$/pAA coacervates and MV. Two cathodic peaks are observed for MV: -682 mV and -594 mV, corresponding to the reduction of MV in solution and in the coacervate phase, respectively. In contrast to the peak at -682 mV, the cathodic current of the peak at -594 mV increases with the number of cycles, due to the gradual accumulation of coacervates on the surface of the electrode. [pAA] = 2 mM (in monomer units), [KKKC] = 1.67 mM, [NaCl] = 100 mM, [MV] = 3.34 mM c) Dissolution of coacervate droplets by reaction with $MV^{\cdot+}$. The formation of $MV^{\cdot+}$ (with a characteristic blue color) can be observed immediately after the application of a 1.5 V potential. After 1 minute, the average coacervate size decreases only in the sample containing MV (panel d), confirming the $MV^{\cdot+}$-mediated mechanism. [pAA] = 4 mM (in monomer units), [KKKC] = 3.34 mM, [NaCl] = 100 mM, [MV] = 6.68 mM. The size of the scale bars is 25 μm. The violin plot in panel d) shows the median (white dot), Q1-Q3 (black box) and Q0-Q4 (black line) for the area (in the micrograph) of 20 coacervate droplets per sample.

Conclusion

Here, we have designed the first electricity-driven system for the transient formation of complex coacervates. By applying a potential between two electrodes in an undivided cell, we were able to drive simultaneous coacervate formation and coacervate dissolution (mediated by an electrocatalyst) in different regions of the cell. Furthermore, the electrochemically-formed coacervates move by electrophoresis in the direction of the electric field, effectively going from the point where they are formed to the point where they are destroyed. Each coacervate moves over a

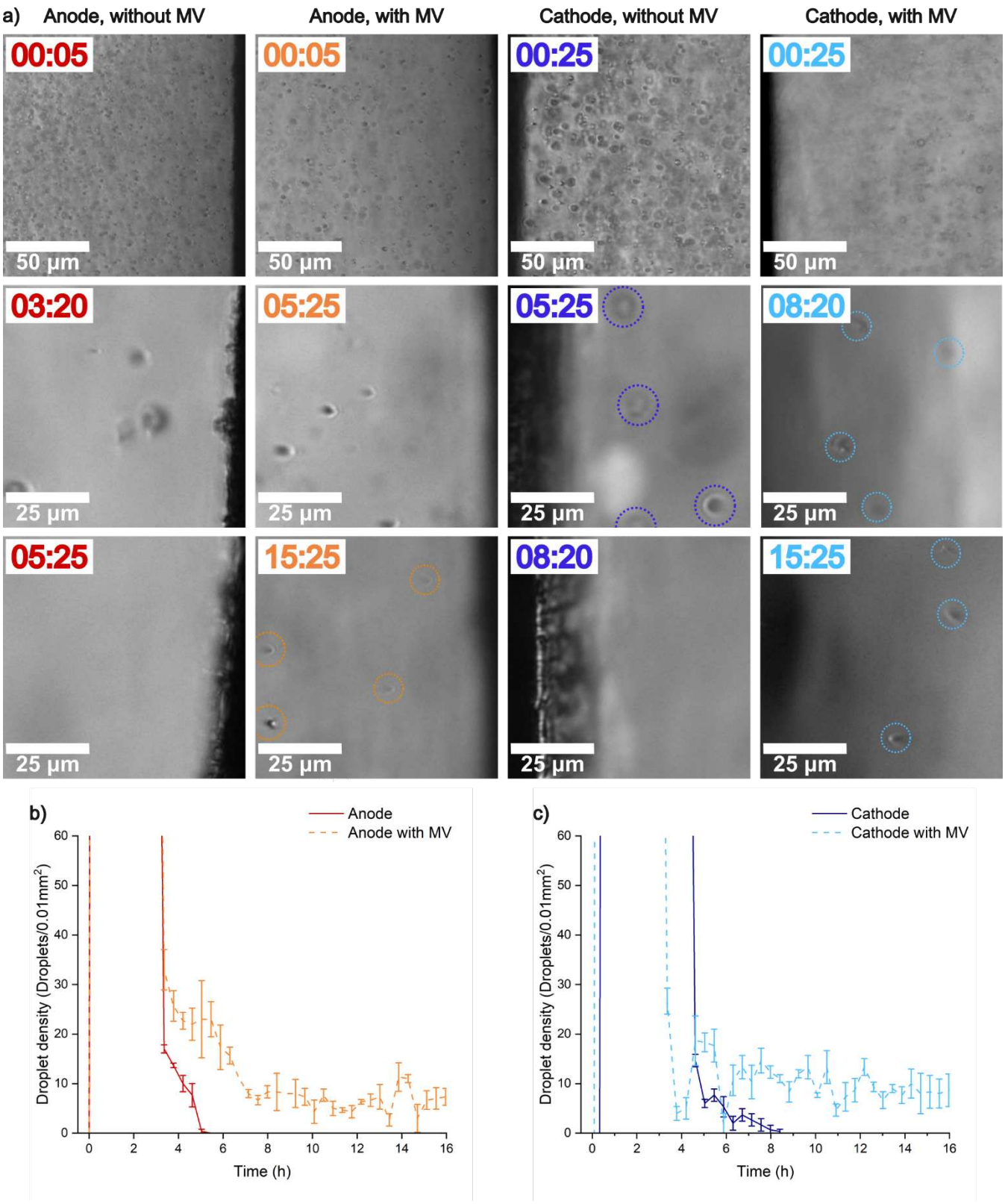


Figure 5. Emergence of a steady state with simultaneous coacervate formation, movement, and destruction. a) Micrographs of $(KKKC)_2$/pAA coacervates next to the anode and cathode, in presence and in absence of MV, at different times after application of the electric potential (0.7 V). The average number of droplets in a 100 x 100 µm area in the proximity of either anode or cathode was counted and plotted against time in panels c) and d). In presence of MV, both the generation of droplets on the anode and the supply of droplets to the cathode can be sustained for several hours, indicating that the system reaches a steady state of formation-movement-destruction. The number of droplets were obtained from manually counting the coacervates droplets in an area of 0.01 mm^2. The data represented corresponds to the average number of three different areas at the same distance from the electrode, and the error bars represent the standard deviation. The number of droplets between 0 and 4 h ($n > 60$) was too high to count manually, but an estimation based on the grey-value of the image can be seen in Figure S11. The size of the scale bar is indicated in the images. Times are reported as hh:mm.

distance of 7.4 mm, over three orders of magnitude larger than their size; and while the lifetime of individual droplets is ~10 minutes, the regime of coacervate formation, movement and destruction can be maintained for more than 16 hours. Sustaining this regime for such a long period of time would have been practically impossible in a chemically-driven system, as the accumulation of ionic side-products in the solution would destabilize the coacervate phase.

The system described here can be used as a starting point to build artificial systems that exhibit coacervate-based active transport. We have shown different molecules to be more soluble inside of the coacervate phase than in the surrounding supernatant, spontaneously being sequestered inside of the droplets. By combining this spontaneous compartmentalization with an electric potential, one can envision coacervate droplets that form in the anode, sequester cargo from their surroundings, and transport it to the cathode, releasing it upon reduction of the coacervate. As long as the coacervate-mediated transport is faster than the diffusion of free solute back to the starting point, this would lead to electrically-driven transport using coacervates as transient carriers, and to the formation of a chemical gradient. Our preliminary data shows that this transport can be selective, and this selectivity could be further enhanced by including specific binding motifs in the sequence of the coacervate-forming peptides.

The system shown here was kept as simple as possible, only including two flat electrodes with a constant electric field between them. However, by combining multiple electrodes in different geometries, more complex systems can be designed, with multiple sources and sinks of coacervate droplets, and complex flows between them.

Experimental section

Materials

Poly(acrylic acid sodium salt) powder (average Mw ~5,100 by GPC), Methyl viologen dichloride hydrate (98%, xH_2O form, three molecules of H_2O per molecule of MV were assumed for the calculations) and Tris hydrochloride (> 99%, pH 7.0-9.0), Rhodamine B, Fluoresceine, Nile Red, Ethylenediaminetetraacetic acid (> 99%) and Ellman's reagent (5,5-dithio-bis-(2-nitrobenzoic acid), > 99%) were purchased from Sigma Aldrich. ATP (Adenosine-5'-triphoshpate disodium salt hydrate, 98%) and Sodium perborate tetrahydrate (97%) were purchased from Alfa Aesar. Sodium chloride (≥ 99.5 %) was purchased from Fisher Chemical. KKKC (trifluoroacetic acid salt, ≥ 95%) was purchased from GenScript Biotech (Rijswijk, The Netherlands). Brooker's merocyanine (1-(6-(Dimethylamino)naphthalen-2-yl)propan-1-one, 95%) was purchased from abcr GmbH (Karlsruhe, Germany).

All samples were prepared using water deionized by reverse osmosis (~ 14 µS/cm).

Optical microscopy was performed on a Nikon Eclipse Ts2 microscope Type 120c in the bright field with 10x, 20x and 40x objectives. All microscope images and videos were analyzed using ImageJ 1.54f.

Preparation of KKKC/pAA and KKKC/ATP solutions

Stock solutions of NaCl (500 mM), KKKC (10 mM), pAA (20 mM in monomer concentration), ATP (10 mM) and MV (400 mM) were prepared in deionized water. To avoid oxidation of KKKC by oxygen in the air, the stock solution of KKKC was bubbled with nitrogen after every use, kept at -20°C and frequently replaced.

The stock solutions were mixed to the desired concentration of each polyelectrolyte and used immediately after preparation. All samples contained Tris buffer (pH = 7.4, 50 mM). The composition of samples was as follows:

- 1:1 KKKC:pAA - 1.34 mM KKKC, 4 mM PAA (monomer concentration), 100 mM NaCl

- 2.5:1 KKKC:pAA - 3.34 mM KKKC, 4 mM PAA (monomer concentration), 100 mM NaCl

- 1:1 KKKC:ATP - 1.34 mM KKKC, 1.34 mM ATP (concentration of charged units), 10 mM NaCl

- 2.5:1 KKKC:ATP - 3.34 mM KKKC, 1.34 mM ATP (concentration of charged units), 10 mM NaCl

In the samples to which MV was added, its concentration was 6.68 mM.

The pH of the samples decreased upon mixing to ~6.5 – 7, due to the TFA in the peptide. The ratios between positive and negative charges were calculated assuming that the ATP bears three negative charges at this pH.

Chemical oxidation of KKKC

The oxidation of KKKC in 1:1 KKKC:pAA and 1:1 KKKC:ATP was performed by the addition of 2.5 eq. of $NaBO_3$ (20 mM solution) to the freshly prepared polyelectrolyte solutions, followed by incubation at room temperature for 45 min.

Electrochemical set-up

For each experiment, a singular well on a 96 well plate with 7.4x7.4 mm square wells (Ibidi) was equipped with flat silver electrodes (2.5 mm width, 0.3 mm thickness). The electric potential was applied by a direct current Laboratory Power Supply EA-PS 3016-10 B (EA Elektro-automatik GmbH & Co. KG). Unless otherwise specified, the applied voltage was 0.7 V.

For the experiments with long measuring times, the well with the electrodes was carefully covered by a piece of a transparent film to prevent water evaporation.

Electrophoretic movement

The displacement of individual droplets was measured by tracking the change of the x coordinate of the center of mass of a circular area corresponding to a coacervate droplet every second for 10 seconds. Typically, tracking an individual droplet for a longer period of time was not feasible, due to the droplet moving out of focus.

Coacervate destruction using an electrocatalytic cycle

Two solutions containing 2.5:1 KKKC:pAA were prepared with and without MV (6.68 mM). In both cases, an electric potential of 0.7 V was applied to the mixture for 15 minutes, until enough coacervate droplets were accumulated in the bottom of the cell next to the cathode. Immediately afterwards, the potential was increased to 1.5 V and the microscope images were recorded within the first 30 seconds and after 1 minute.

The size distribution of the droplets before and after application of the 1.5 V electric potential were obtained from measuring the area of the droplets next to the cathode. For each image, 20 droplets were measured and the dataset was used to generate the grouped violin graph shown in Figure 4.

Steady state experiments

Two different methods were used to estimate the number of coacervate droplets over the course of long experiments. For the “droplet density” estimation (See Figure S8), the images were converted to grayscale, and the mean gray values in an area of 0.01 mm^2 next to the corresponding electrode were measured. The data was normalized by the initial value before the coacervates had started forming. The relative droplet density was estimated by inversion of the relative mean gray value, setting the initial value as 0. For the direct counting, a square area of 100x100 µm was selected close to the electrode, and the droplets inside it were manually counted for frames separated by 25.2 min.

In both cases, the count was repeated three times in different areas at the same distance from to the electrode in the upper, middle and lower part of the image.

Supporting Information

The following files are available as Supporting information:

Controls of electrochemical coacervate formation, additional characterization by cyclic voltammetry, NMR, UV and fluorescent microscopy (PDF);

Supplementary Video 1, showing the real-time electrophoretic movement of coacervates with different compositions (MP4);

Supplementary Video 2, showing the time-lapses recorded next to the anode and cathode for samples with and without MV (MP4).

Acknowledgements

The authors would like to thank V. Badets, A. Jouaiti, and A. Fluck for helpful assistance with cyclic voltammetry, F. Rahmatova, C. Bonfio, D. Ndiaye and P. Faller for assistance with peptide synthesis in preliminary studies, Y. Geiger for proofreading the manuscript and giving useful suggestions, and E. Elovaya for stimulating discussions.

This work has benefitted from support provided by the University of Strasbourg Institute for Advanced Study (USIAS) for a Fellowship, within the French national program “Investment for the future” (IdEx-Unistra). S. S. and G. M. S. also acknowledge support from the program “Attractivité” of the framework “IdEx University of Strasbourg”. K. F. thanks the CSC Graduate School funded by the French National Research Agency (CSC-IGSANR-17-EURE-0016) for a Master fellowship. L. C. R. acknowledges the support of the Spanish Ministry of Science, Innovation and Universities (MICIU) for a FPI predoctoral fellowship (No. PRE2020-095493).

Keywords: active coacervates, transient formation, electricity-driven, waste-free

[1] K. Ruiz-Mirazo, C. Briones, A. De La Escosura, *Open Biology* **2017**, *7*, 170050.
[2] L. Leon, G. M. Santiago, E. Spruijt, *Commun. Chem.* **2024**, *7*, 275, s42004-024-01358–1.
[3] E. Penocchio, A. Bachir, A. Credi, R. D. Astumian, G. Ragazzon, *Chem* **2024**, S2451929424003814.
[4] S. Matsumura, Á. Kun, M. Ryckelynck, F. Coldren, A. Szilágyi, F. Jossinet, C. Rick, P. Nghe, E. Szathmáry, A. D. Griffiths, *Science* **2016**, *354*, 1293–1296.
[5] E. D. Gundelfinger, M. M. Kessels, B. Qualmann, *Nat. Rev. Mol. Cell Biol.* **2003**, *4*, 127–139.
[6] L.-G. Wu, E. Hamid, W. Shin, H.-C. Chiang, *Annu. Rev. Physiol.* **2014**, *76*, 301–331.
[7] S. F. Banani, H. O. Lee, A. A. Hyman, M. K. Rosen, *Nat Rev Mol Cell Biol* **2017**, *18*, 285–298.
[8] E. Gomes, J. Shorter, *J. Biol. Chem.* **2019**, *294*, 7115–7127.
[9] I. A. Antifeeva, A. V. Fonin, A. S. Fefilova, O. V. Stepanenko, O. I. Povarova, S. A. Silonov, I. M. Kuznetsova, V. N. Uversky, K. K. Turoverov, *Cell. Mol. Life Sci.* **2022**, *79*, 251.
[10] B. Portz, J. Shorter, *J. Mol. Biol.* **2021**, *433*, 166794.
[11] M. Hondele, S. Heinrich, P. De Los Rios, K. Weis, *Emerg. Top. Life Sci.* **2020**, *4*, 343–354.
[12] W. M. Aumiller, F. Pir Cakmak, B. W. Davis, C. D. Keating, *Langmuir* **2016**, *32*, 10042–10053.
[13] N. A. Yewdall, A. A. M. André, T. Lu, E. Spruijt, *Curr. Opin. Colloid Interface Sci.* **2021**, *52*, 101416.
[14] S. Cao, T. Ivanov, J. Heuer, C. T. J. Ferguson, K. Landfester, L. Caire Da Silva, *Nat. Commun.* **2024**, *15*, 39.
[15] A. M. Rumyantsev, N. E. Jackson, J. J. de Pablo, *Annu. Rev. Condens. Matter Phys.* **2021**, *12*, 155–176.
[16] C. E. Sing, S. L. Perry, *Soft Matter* **2020**, *16*, 2885–2914.
[17] B. Wang, T. O. Akanbi, D. Agyei, B. J. Holland, C. J. Barrow, in *Role of Materials Science in Food Bioengineering* (Eds.: A.M. Grumezescu, A.M. Holban), Academic Press, **2018**, pp. 235–261.
[18] C. Forenzo, J. Larsen, *Mol. Pharmaceutics* **2023**, *20*, 4387–4403.
[19] I. B. A. Smokers, B. S. Visser, A. D. Slootbeek, W. T. S. Huck, E. Spruijt, *Acc. Chem. Res.* **2024**, 57, 1885–1895.
[20] A. Sanchez-Fernandez, I. Insua, J. Montenegro, *Commun. Chem* **2024**, *7*, 223.
[21] W. M. Aumiller, C. D. Keating, *Nat. Chem.* **2016**, *8*, 129–137.
[22] C. Donau, F. Späth, M. Sosson, B. A. K. Kriebisch, F. Schnitter, M. Tena-Solsona, H.-S. Kang, E. Salibi, M. Sattler, H. Mutschler, J. Boekhoven, *Nat. Commun.* **2020**, *11*, 5167.
[23] M. Abbas, W. P. Lipiński, J. Wang, E. Spruijt, *Chem. Soc. Rev.* **2021**, *50*, 3690–3705.
[24] K. K. Nakashima, M. H. I. van Haren, A. A. M. André, I. Robu, E. Spruijt, *Nat. Commun.* **2021**, *12*, 3819.
[25] T. P. Fraccia, N. Martin, *Nat. Commun.* **2023**, *14*, 2606.
[26] H. Seo, H. Lee, *Adv. Sci.* **2024**, *11*, 2305760.
[27] K. K. Nakashima, J. F. Baaij, E. Spruijt, *Soft Matter* **2018**, *14*, 361–367.
[28] S. Sharma, A. Belluati, M. Kumar, S. Dhiman, *Angew. Chem. Int. Ed.* **2024**, e202421620.
[29] W. Liu, J. Deng, S. Song, S. Sethi, A. Walther, *Commun. Chem.* **2024**, *7*, 1–10.
[30] C. Donau, J. Boekhoven, *Trends Chem.* **2023**, *5*, 45–60.
[31] A. M. Bergmann, J. Bauermann, G. Bartolucci, C. Donau, M. Stasi, A.-L. Holtmannspötter, F. Jülicher, C. A. Weber, J. Boekhoven, *Nat. Commun.* **2023**, *14*, 6552.
[32] J. Boekhoven, J. Sastre, A. Thatte, A. Bergmann, M. Stasi, M. Tena-Solsona, C. Weber, *Nat. Commun.* **2025**, 16, 2003.
[33] L. Yan, W. Zheng, E. Muller, P. Carl, T. M. Hermans, G. M. Santiago, *Macromolecules* **2025**, 58, 3635–364.
[34] X. Chen, H. Soria-Carrera, O. Zozulia, J. Boekhoven, *Chem. Sci.* **2023**, *14*, 12653–12660.
[35] A. Sorrenti, J. Leira-Iglesias, A. J. Markvoort, T. F. A. De Greef, T. M. Hermans, *Chem. Soc. Rev.* **2017**, *46*, 5476–5490.
[36] G. Ragazzon, M. Malferrari, A. Arduini, A. Secchi, S. Rapino, S. Silvi, A. Credi, *Angew. Chem. Int. Ed*. **2023**, *62*, e202214265.
[37] D. Barpuzary, P. J. Hurst, J. P. Patterson, Z. Guan, *J. Am. Chem. Soc.* **2023**, *145*, 3727–3735.
[38] J. Wang, M. Abbas, J. Wang, E. Spruijt, *Nat. Commun.* **2023**, *14*, 8492.
[39] J. Wang, M. Abbas, Y. Huang, J. Wang, Y. Li, *Commun. Chem.* **2023**, *6*, 1–8.
[40] Y. Yin, L. Niu, X. Zhu, M. Zhao, Z. Zhang, S. Mann, D. Liang, *Nat. Commun*. **2016**, *7*, 10658.
[41] Z. Liu, J. Chen, Q. Bai, Y. Lin, D. Liang, *Langmuir* **2022**, *38*, 6425–6434.
[42] M. H. I. van Haren, B. S. Visser, E. Spruijt, *Nat. Commun.* **2024**, *15*, 3564.
[43] A. Agrawal, J. F. Douglas, M. Tirrell, A. Karim, *Proc. Natl. Acad. Sci.* **2022**, *119*, e2203483119.
[44] Y. Kim, Y. Zheng, *Nano Lett.* **2024**, *24*, 15964–15972.

[45] These solutions were not degassed, and therefore dissolved oxygen can act as a sacrificial electron acceptor for the electrochemical oxidation of KKKC. In the final system, the reduction of MV acts as a counter-reaction to the oxidation of KKKC. For the reduction of O_2 on a silver surface, see: M. Innocenti, C. Zafferoni, A. Lavacchi, L. Becucci, F. Di Benedetto, E. Carretti, F. Vizza, M. L. Foresti, *J. Electrochem. Soc.* **2014**, 161, D3018–D3024.
[46] N. S. Lawrence, J. Davis, R. G. Compton, *Talanta* **2001**, *53*, 1089–1094.
[47] X. Liu, H. Lv, Q. Sun, Y. Zhong, J. Zhao, J. Fu, M. Lin, J. Wang, *Anal. Lett.* **2012**, *45*, 2246–2256.
[48] Y. Wen, L. Pei, T. Wei, *Mat. Res.* **2017**, *20*, 592–600.
[49] S. Selmani, E. Schwartz, J. T. Mulvey, H. Wei, A. Grosvirt-Dramen, W. Gibson, A. I. Hochbaum, J. P. Patterson, R. Ragan, Z. Guan, *J. Am. Chem. Soc.* **2022**, *144*, 7844–7851.
[50] J. C. Love, L. A. Estroff, J. K. Kriebel, R. G. Nuzzo, G. M. Whitesides, *Chem. Rev.* **2005**, *105*, 1103–1170.
[51] L. Shang, S. Dong, *Biosens. Bioelectron.* **2009**, *24*, 1569–1573.
[52] W. Leesutthiphonchai, W. Dungchai, W. Siangproh, N. Ngamrojnavanich, O. Chailapakul, *Talanta* **2011**, *85*, 870–876.

Supplementary Files

This is a list of supplementary files associated with this preprint. Click to download.

- 20250707SI.pdf
- SupportingVideo1.mp4
- SupportingVideo2smaller.mp4